water

MDPI

Article

A Study on the Hydrochemical Evolution Property and Pollution Source Attribution of Groundwater in Highly Urbanized Areas: A Case Study of Shenzhen City

Yue Wei [1], Yang Li [2], Lihong Zhang [1], Chuane Liu [1], Qingzhai Meng [1], Jianbo Yin [1,*] and Long Wang [3]

[1] 801 Institute of Hydrogeology and Engineering Geology, Shandong Provincial Bureau of Geology and Mineral Resources (SPBGM), Jinan 250014, China
[2] Land and Resources Exploration Center of Hebei Bureau of Geology and Mineral Resources Exploration (Hebei Mining and Geological Disaster Emergency Rescue Center), Shijiazhuang 050061, China
[3] Chinese Academy of Geological Sciences, Beijing 100037, China
* Correspondence: jianbo2025524@163.com

Abstract

Accurate identification of groundwater pollution sources is crucial for the socio-economic development of a region. In highly urbanized areas, where human activities have a pronounced impact on groundwater, however, the hydrochemical evolution patterns and sources of pollutants remain unclear. Taking Shenzhen, a highly urbanized city in China, as a case study, this research employed a combination of multivariate statistical techniques and the Positive Matrix Factorization (PMF) model to elucidate the hydrochemical evolution and quantitatively parse the pollution sources of groundwater in such regions. The results revealed that the pH of groundwater in the study area ranged from 4.24 to 7.31, indicating weak acidity to neutrality. The exceedance rates for pH, NH_4^+, COD, Mn, and Fe were as high as 67.1%, 44.3%, 44.3%, 34.3%, and 31.4%, respectively. The Water Quality Index assessment revealed that 32.9% of the groundwater samples were classified as poor, highlighting the significant impact of human activities. Land-use types significantly affected groundwater quality, with urban areas exhibiting higher concentrations of the COD, NO_3^-, Mn, and Fe compared to agricultural and forested areas. The predominant hydrochemical type of groundwater in the study area was HCO_3·Cl—Ca·Na, with rock weathering (primarily silicate weathering) being the dominant process controlling groundwater chemistry. The PMF model identified three major pollution sources in the highly urbanized region: domestic and industrial wastewater, enhanced water-rock interactions leading to the release of hydrochemical components, and agricultural fertilizers, contributing 43.9%, 37.0%, and 19.1% to groundwater pollution, respectively. Geostatistical spatial interpolation techniques demonstrated that in urban areas, groundwater quality was primarily controlled by the discharge of domestic and industrial wastewater, while in agricultural areas, excessive fertilizer application was the main driver of groundwater degradation. These findings provide a scientific basis for groundwater pollution prevention and sustainable utilization in highly urbanized regions.

Keywords: urbanization; groundwater; pollution source apportionment; PMF model; land use

Academic Editor: Pankaj Kumar

Received: 10 September 2025
Revised: 2 October 2025
Accepted: 10 October 2025
Published: 13 October 2025

Citation: Wei, Y.; Li, Y.; Zhang, L.; Liu, C.; Meng, Q.; Yin, J.; Wang, L. A Study on the Hydrochemical Evolution Property and Pollution Source Attribution of Groundwater in Highly Urbanized Areas: A Case Study of Shenzhen City. *Water* **2025**, *17*, 2945. https://doi.org/10.3390/w17202945

1. Introduction

As one of the world's most vital freshwater resources, groundwater accounts for approximately 96% of the planet's total freshwater reserves. It serves not only as a crucial

source of drinking water for numerous regions but also plays an essential role in agricultural irrigation and industrial water use [1–3]. In arid and semi-arid areas, groundwater often represents the sole reliable water supply [4]. However, the increasing global population and rapid urbanization have led to a continuous rise in groundwater extraction and utilization. Concurrently, human activities have intensified the impact on groundwater quality [5,6]. Groundwater contamination poses a threat not only to the safety of drinking water but also to human health and ecosystems through its use in irrigation and industry [7–9]. Thus, accurately identifying the sources of groundwater pollution has become of paramount importance.

In recent years, the issue of groundwater contamination has garnered increasing attention, with notable advancements in the identification of pollution sources both domestically and internationally. Traditionally, the identification of groundwater pollution sources has primarily relied on chemical analysis methods, which involve measuring the concentrations of various pollutants in groundwater and utilizing ratios between different water chemical components to identify pollution sources [10,11]. However, this approach faces limitations when dealing with complex pollution sources, as it struggles to accurately differentiate pollutants from various origins. Some scholars have employed periodic sampling and detection in conjunction with multivariate statistical techniques, such as correlation analysis and principal component analysis, to qualitatively identify the sources of pollutants in groundwater [12]. Nevertheless, these multivariate statistical techniques fail to accurately quantify the contribution rates of individual pollution sources [13]. In recent years, the Positive Matrix Factorization (PMF) model, developed by the U.S. Environmental Protection Agency, has been widely applied in source apportionment studies of atmospheric, soil, and surface water environments [14,15]. This model not only accurately identifies the sources of pollutants in the environment but also quantifies the contribution rates of each pollution source to the entire study area and the monitoring sites [16,17], thereby enhancing the efficiency of source tracing. Although the PMF model is widely used in other environmental media, its application to identify groundwater pollution sources, especially in highly urbanized areas with multiple pollution sources, remains limited.

The groundwater systems in urbanized regions are influenced by both geological structures and human activities, such as industrial production, agricultural practices, urban construction, and domestic wastewater discharge. These influences lead to significant variations in the recharge, flow, and discharge mechanisms across different areas, resulting in complex and dynamically changing pollution sources [18]. Therefore, investigating the sources of groundwater pollution in highly urbanizing areas holds great scientific significance and practical application value. Shenzhen, located in the Pearl River Delta, is a highly developed and densely populated modern city. With the acceleration of urbanization, the city's groundwater system is under multiple pressures. On one hand, urbanization has increased impervious surfaces, altering the recharge conditions of groundwater [19]. On the other hand, human activities like industrial production, agricultural practices, and domestic wastewater discharge have significantly heightened the risk of groundwater contamination [20]. At present, systematic studies on the sources of groundwater pollution in Shenzhen are still lacking. Most research has focused on the current status and extent of groundwater quality, with insufficient in-depth analysis of the dynamic changes in pollution sources [21,22]. This limitation makes it difficult to fully understand the complex pollution sources. Thus, conducting a comprehensive study on the sources of groundwater pollution in Shenzhen is of great scientific and practical significance.

This study systematically investigates the hydrochemical evolution and pollution sources of groundwater in Shenzhen by integrating a suite of techniques, including chemical analysis, multivariate statistical techniques, the PMF model, and GIS spatial interpolation.

The research focuses on three main aspects: (1) the characteristics and assessment of groundwater quality in highly urbanized areas; (2) the hydrochemical evolution patterns of groundwater in these regions; and (3) the quantitative identification of groundwater pollution sources. The findings are expected to provide crucial insights for groundwater protection and pollution control in rapidly urbanizing areas.

2. Materials and Methods

2.1. Study Area

2.1.1. Overview of the Study Area

Shenzhen is a modern international metropolis situated in the southern part of Guangdong Province, China. It lies on the eastern shore of the Pearl River estuary, borders Daya Bay and Dapeng Bay to the east, fronts the Pearl River estuary and Lingdingyang to the west, adjoins Hong Kong along the Shenzhen River to the south, and abuts Dongguan and Huizhou to the north. The city is located south of the Tropic of Cancer between longitudes 113°43′–114°38′ E and latitudes 22°24′–22°52′ N, covering a total area of 1997.47 km^2. The multi-year mean annual air temperature is 23 °C, and the multi-year mean annual precipitation is 1935.8 mm, with an average of 131 rainy days per year. Among them, farmland accounts for 7.65%, urban and rural land accounts for 24.3%, forest and grassland account for 64.1%, and water area accounts for 3.95%.

Rapid socio-economic development in recent decades has made Shenzhen one of China's most urbanized cities, with an urbanization rate approaching 100%. Its industrial activities include high-tech industries, advanced manufacturing, traditional manufacturing, electroplating, printed circuit board manufacturing, chemical industry, textile and dyeing industry, papermaking industry, and food processing, among others. Concomitant growth in industrial and agricultural water demand has exerted substantial pressure on groundwater quality.

2.1.2. Geological and Hydrogeological Conditions

Shenzhen lies within the hydrogeological sub-region of the Pearl River Delta. Exposed strata in the area comprise mainly the Lower Paleozoic, Middle and Upper Devonian, Carboniferous, Jurassic, Cretaceous, Tertiary and Quaternary systems. Structural features are well developed; NE-trending structures predominate, followed by NW-trending and E–W-trending structures, with minor N–S-trending faults sporadically exposed. Quaternary deposits are widespread, consisting predominantly of alluvial layers along riverbanks, fluvio-marine deltaic sequences at estuaries, and marine deposits along the coastal zone.

Groundwater in Shenzhen can be classified into three types: pore water in unconsolidated Quaternary sediments, fissure water in bedrock, and karst water. The primary recharge sources are atmospheric precipitation and lateral inflow from rivers. In addition, groundwater can also be replenished through human-made structures such as reservoirs, agricultural irrigation systems, and ponded water in pits. Groundwater flow is controlled by topography, generally moving from mountainous or hilly areas toward valley basins, ultimately discharging southward into the sea or northward into Dongguan and Huizhou. Discharge mechanisms include spring outflow, baseflow to surface water bodies, evaporation and artificial abstraction.

2.2. Sample Collection and Analysis

2.2.1. Acquisition of Groundwater Samples

Groundwater samples were collected during June–July 2021. A total of 70 samples were obtained exclusively from domestic wells; their spatial distribution is shown in Figure 1. Prior to sampling, bottles were rinsed with deionized water; immediately before

collection, each bottle was conditioned by rinsing three times with the groundwater to be sampled to ensure cleanliness. After collection, samples were placed in portable refrigerated coolers, transported to the laboratory, filtered through 0.45 μm membranes, and stored in 500 mL polyethylene bottles. Aliquots designated for cation analysis were acidified to pH < 2 using 1:1 HNO_3.

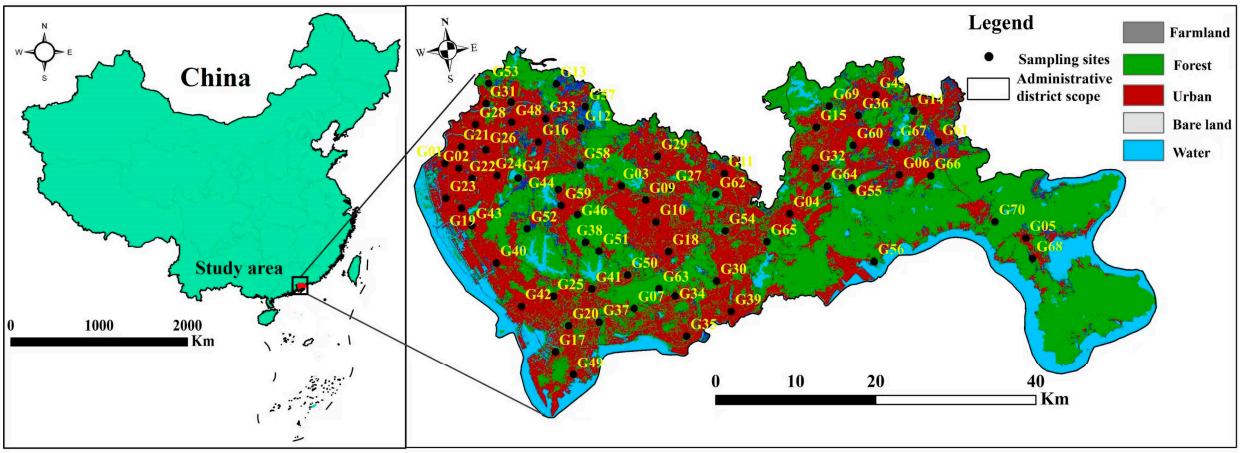

Figure 1. Distribution Map of Sampling Sites.

2.2.2. Hydrochemical Analysis

Measured parameters comprised field-determined pH and dissolved oxygen (DO), together with laboratory analyses for K^+, Na^+, Ca^{2+}, Mg^{2+}, Cl^-, $SO_4{}^{2-}$, $HCO_3{}^-$, $NO_3{}^-$, $NO_2{}^-$, $NH_4{}^+$, chemical oxygen demand (COD), total hardness (TH), total dissolved solids (TDS), Fe, and Mn. Analytical methods, instrumentation, and method detection limits for each hydrochemical variable are summarized in Supplementary Table S1.

2.2.3. Analysis of Data

Water Quality Index (WQI) Approach

The Water Quality Index is a widely recognized tool for assessing groundwater quality and its suitability for drinking purposes. In the WQI calculation, each hydrochemical parameter is assigned a weight (W_i) that reflects its relative importance to overall groundwater quality. The present study adopts the Class III thresholds prescribed by the Chinese "Standard for Groundwater Quality" (GB/T 14848-2017) [23] as the primary reference; where a parameter is not included in that standard, the guideline value given by the World Health Organization (WHO, 2011) [24] is used instead.

The procedural steps for computing *WQI* are summarized below:

$$W_i = \frac{W_i}{\sum_{i=1}^{n} W_i}$$

$$Q_i = {}^{C_i}/_{S_i} \times 100$$

$$SI_j = W_i \times Q_i$$

$$WQI = \sum SI_j$$

where Q_i denotes the quality rating; C_i and S_i denote the concentration (mg/L) and the water quality standard of each indicator, respectively; and SI_j is the sub-index of the i-th indicator. The specific values of the weights assigned to each water chemistry index are detailed in Supplementary Table S2.

Positive Matrix Factorization (PMF) Model

The PMF model, recommended by the United States Environmental Protection Agency, is a receptor-oriented source-apportionment technique. By decomposing the sample-variable matrix into factor contributions and profiles through non-negativity constraints on both matrices, PMF reduces high-dimensional hydrochemical data to a small number of latent factors without requiring prior source-composition spectra. Owing to its operational simplicity and robustness, the method has been extensively applied to atmospheric, soil, and aquatic environmental systems.

The model computation is expressed as Equation:

$$X_{ij} = \sum_{k=1}^{p} g_{ik} f_{ki} + e_{ij}$$

where X_{ij}: Concentration of species j in sample i; g_{ik}: Contribution of source k to sample i; f_{kj}: Concentration of species j in source k; and e_{ij}: Residual, i.e., the portion of X<sub> not explained by the PMF model. PMF iteratively decomposes the original data matrix to obtain the optimal matrices G and F by minimizing the objective function Q.

Spatial Interpolation

Spatial interpolation is a fundamental technique in geographic information systems (GIS) and spatial analysis that estimates values at unsampled locations from point observations. In water-quality studies, it is routinely employed to map pollutant concentrations, water temperature, bathymetry, and other variables. Kriging-an optimal geostatistical interpolator-exploits spatial autocorrelation by fitting a semivariogram model to the data; it minimizes the estimation variance while preserving the spatial structure of the variable. Beyond yielding accurate, smooth prediction surfaces, Kriging also quantifies the uncertainty of each estimate. In the present work, Kriging was applied to project the source contributions obtained from the PMF model onto the study-area basemap, thereby visualizing the spatial distribution of contaminant sources across Shenzhen.

Multivariate Statistical Techniques

To assess the variations in groundwater quality among different land-use types, the nonparametric Kruskal–Wallis test was utilized, with a significance level set at $p < 0.05$. Subsequently, pairwise comparisons between the three groups were carried out using the Mann–Whitney U test. The R computing platform was employed to perform all statistical analyses (version 4.3.2 (New Zealand)).

Chloro-Alkaline Indices (CAI)

To elucidate the chemical evolution process of groundwater, we utilized *CAI* to evaluate the cation exchange among its chemical constituents.

$$CAI - 1 = \frac{\left[\gamma\left(Na^{+}\right) + \gamma\left(K^{+}\right)\right] - \gamma\left(Cl^{-}\right)}{\gamma\left(Cl^{-}\right)}$$

$$CAI - 2 = \frac{\left[\gamma\left(Na^{+}\right) + \gamma\left(K^{+}\right)\right] - \gamma\left(Cl^{-}\right)}{\gamma\left(SO_4^{2-}\right) + \gamma\left(HCO_3^{-}\right) + \gamma\left(CO_3^{2-}\right)}$$

3. Results

3.1. Properties of Groundwater Hydrochemistry

To thoroughly assess the groundwater quality within the study area, a detailed statistical analysis was performed on the hydrochemical parameters obtained from all sampling points. The compiled data for each chemical parameter can be found in Table 1. Groundwater pH across the study area ranges from 4.24 to 7.31, with a mean of 6.08; 67.1% of the samples fall below the national Class III threshold (pH < 6.5), indicating a predominantly weakly acidic to neutral signature. Previous studies have found that the frequency of acid rain in the Shenzhen area is as high as 70%, with an average pH value of 4.25. Therefore, acidic precipitation could be an important reason for the low pH of groundwater [25]. Dissolved-oxygen (DO) concentrations vary between 0.950 and 8.19 mg/L (mean value is 2.85 mg/L); The low concentration of DO is closely related to the shallow depth of groundwater and its susceptibility to human activities [26]. Cation abundances follow the order Ca^{2+} (46.5 mg/L) > Na^{+} (46.0 mg/L) > K^{+} (21.9 mg/L) > Mg^{2+} (5.22 mg/L) > NH_4^{+} (4.78 mg/L). NH_4^{+} exceeds the Class III limit in 44.3% of the samples, evidencing pronounced anthropogenic inputs. Anion abundances decrease as HCO_3^{-} (158 mg/L) > Cl^{-} (66.7 mg/L) > SO_4^{2-} (39.5 mg/L) > NO_3^{-} (31.3 mg/L) > NO_2^{-} (1.94 mg/L); NO_2^{-} and NO_3^{-} surpass the respective thresholds in 14.3% and 10.0% of the samples, further confirming intensive human impact. Chemical oxygen demand (COD) ranges from 0.530 to 47.3 mg/L (mean 5.37 mg/L), with an exceedance rate of 44.3%. The wide concentration span and high non-compliance rate stem from domestic and industrial effluents, agricultural non-point sources, and heterogeneities in hydrogeological settings. Mean Fe and Mn concentrations are 0.992 and 0.278 mg/L, respectively, with exceedance rates of 31.4% and 34.3%. Overall, the exceedance rate of groundwater chemical components in highly urbanized areas is higher than that in areas with lower levels of urbanization, such as riparian zones and agricultural areas [27,28]. This further indicates that the groundwater quality in highly urbanized areas has been strongly affected by human activities.

Table 1. Statistical table of hydrochemical components of groundwater in the study area.

Parameters	Units	Range	Mean	SD	Standard	Exceed Standards for All Sites (%)
pH	—	4.24–7.31	6.08	0.678	6.5~8.5	67.1
DO	mg/L	0.950–8.19	2.85	1.43	—	—
TDS	mg/L	44.8–1906	465	424	≤1000	12.9
K^{+}	mg/L	0.26–104	21.3	25.5	—	—
Na^{+}	mg/L	2.91–342	46.0	51.1	≤200	1.43
Ca^{2+}	mg/L	3.19–247	46.5	46.6	—	—
Mg^{2+}	mg/L	0–23.2	5.22	4.57	—	—
NH_4^{+}	mg/L	0–45.0	4.78	10.2	≤0.643	44.3
Cl^{-}	mg/L	3.57–496	66.7	74.3	≤250	2.86
SO_4^{2-}	mg/L	0.142–295	39.5	47.0	≤250	1.43
HCO_3^{-}	mg/L	6.04–673	158	173	—	—
NO_3^{-}	mg/L	0.662–185	31.3	37.5	≤88.6	10.0
NO_2^{-}	mg/L	0.003–33.2	1.94	5.71	≤3.29	14.3
TH	mg/L	13.8–617	142	125	≤450	1.43
Mn	mg/L	0.003–2.96	0.278	4.75	≤0.1	34.3
Fe	mg/L	0–11.5	0.992	36.5	≤0.3	31.4
COD	mg/L	0.530–47.3	5.37	23.2	≤3	44.3

Note: The Standard Refers to the Class III Standard of the Chinese Groundwater Quality Standard (GB/T 14848-2017) [23].

3.2. Types of Groundwater Hydrochemistry

Piper diagrams were employed to delineate the hydrochemical facies, dominant ion assemblages, and evolutionary trends of groundwater within the study area. As illustrated in Figure 2, samples were classified according to the Shukalev scheme. Carbonate alkalinity (HCO_3^-) predominates among anions, whereas sodium (Na^+) constitutes the principal cation. Thirteen distinct hydrochemical types were identified; the four most prevalent are HCO_3·Cl–Ca·Na (50.0%), HCO_3·SO_4·Cl–Ca·Na (12.9%), HCO_3–Ca·Na (10.0%), and HCO_3·Cl–Ca (7.14%). Notably, Cl^-, Na^+, and SO_4^{2-} appear in 82.9%, 85.7%, and 20.0% of the facies designations, respectively—an unambiguous signal of anthropogenic modification of the groundwater system.

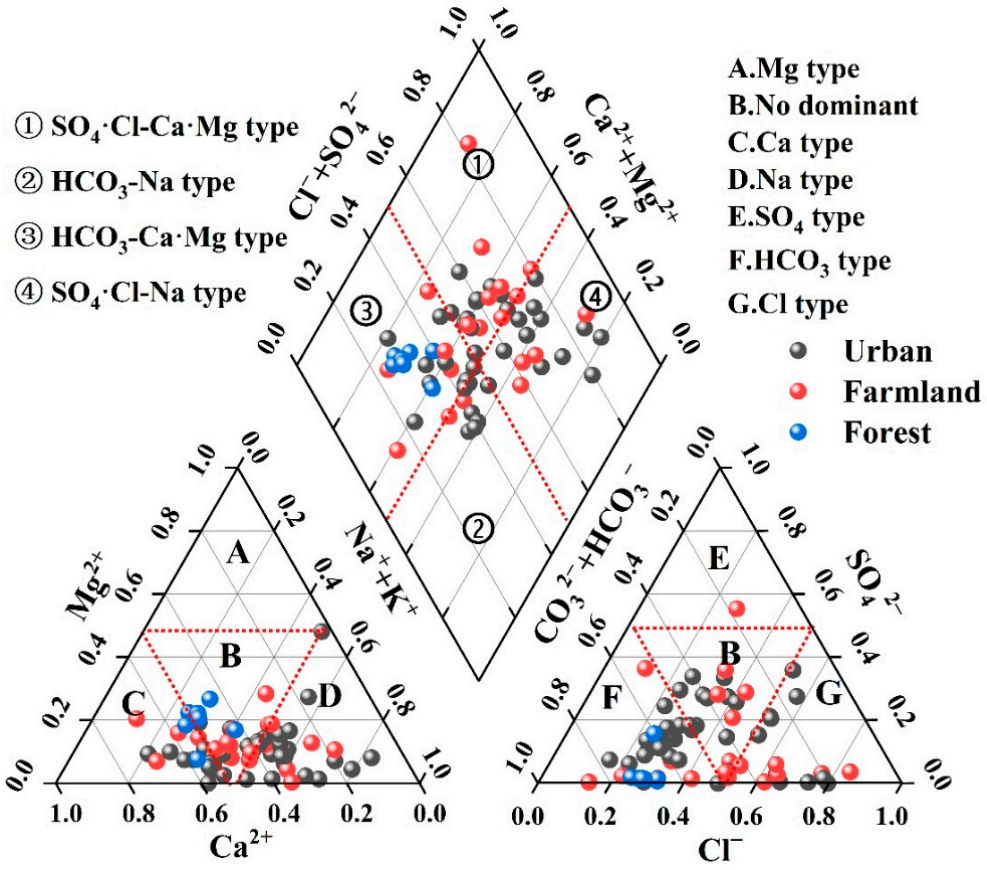

Figure 2. Hydrochemical Types of Groundwater.

3.3. Water Quality Assessment by Using WQI Methods

The WQI was applied to assess groundwater potability across the study area (Table 2). Of the sampled sites, 60.0% were classified as "excellent", 7.1% as "good", whereas 4.3% were rated "poor" and a further 4.3% as "very poor". Approximately 24.3% of the stations yielded water deemed "unsuitable for drinking". Significantly, all non-potable sites are located within urban land-use zones, highlighting that rapid urbanization and the associated anthropogenic pressures are the primary drivers of groundwater quality degradation [29].

Table 2. Statistics of water quality assessment results.

Water Quality Level	Comprehensive Water Quality Score	Monitoring Stations	Proportion (%)	Urban (%)	Forest (%)	Farmland (%)
Excellent water	<50	42	60.0%	24.29%	14.3%	21.4%
Good water	50–100	5	7.14%	4.29%	—	2.86%
Poor water	100.1–200	3	4.29%	4.29%	—	—
Very poor water	200.1–300	3	4.29%	2.86%	—	1.43%
Water unsuitable for drinking purposes	>300	17	24.3%	24.3%	—	—

4. Discussion

4.1. Influence of Land-Use Type on Groundwater Hydrochemistry

Land-use type serves as a direct proxy for the intensity and nature of anthropogenic disturbance, and pollutant sources differ markedly among urban, agricultural, and forested areas. Previous studies have documented that urban zones usually exhibit elevated concentrations of heavy metals (e.g., Fe and Mn) and organic contaminants such as polycyclic aromatic hydrocarbons, primarily because of untreated or partially treated industrial effluents and domestic sewage. Agricultural regions, in contrast, are characterized by high NO_3^- and NH_4^+ levels derived from intensive fertilizer and pesticide application. Forested catchments, benefiting from natural attenuation and minimal human interference, generally display the lowest contaminant burdens [30].

In this study, six hydrochemical indicators (pH, DO, COD, NO_3^-, Cl^-, and Mn) were selected to quantify the impact of land-use on groundwater quality (Figure 3). As depicted in Figure 3a, the mean pH of groundwater in urban areas (6.24) is significantly higher than that in agricultural areas (5.77) ($p < 0.05$). Previous studies have demonstrated that the majority of rainfall in this region is acidic, with a mean pH value of 4.25 [25]. This difference is attributed to the extensive impervious surfaces in urban areas, which prevent acidic precipitation from directly infiltrating the aquifer [5], whereas in agricultural fields, acid rain can percolate immediately, depressing groundwater pH.

COD concentrations in urban groundwater (6.13 mg/L) are significantly elevated relative to forest sites (1.97 mg/L) (Figure 3b). Likewise, NO_3^- in urban groundwater (43.8 mg/L) exceeds that in agricultural (19.1 mg/L, $p < 0.01$) and forest (8.87 mg/L, $p < 0.001$) groundwater; the difference between agricultural and forest samples is not statistically significant ($p > 0.05$) (Figure 3c). These patterns confirm that domestic and industrial effluents are the dominant nitrate source in urban aquifers, consistent with the findings of Zhang et al. [31].

Cl^- and Mn concentrations are also significantly higher in urban (79.5 and 0.288 mg/L) and agricultural (68.4 and 0.380 mg/L) groundwater than in forest groundwater (13.1 and 0.026 mg/L) (Figure 3d,e). Conversely, DO is markedly higher in forest groundwater (4.49 mg/L) than in urban or agricultural groundwater (both 2.58 mg/L) ($p < 0.001$) (Figure 3f). This is primarily because forestry land is mostly situated in mountainous areas, distant from human settlements, which results in weaker human impacts on the local groundwater.

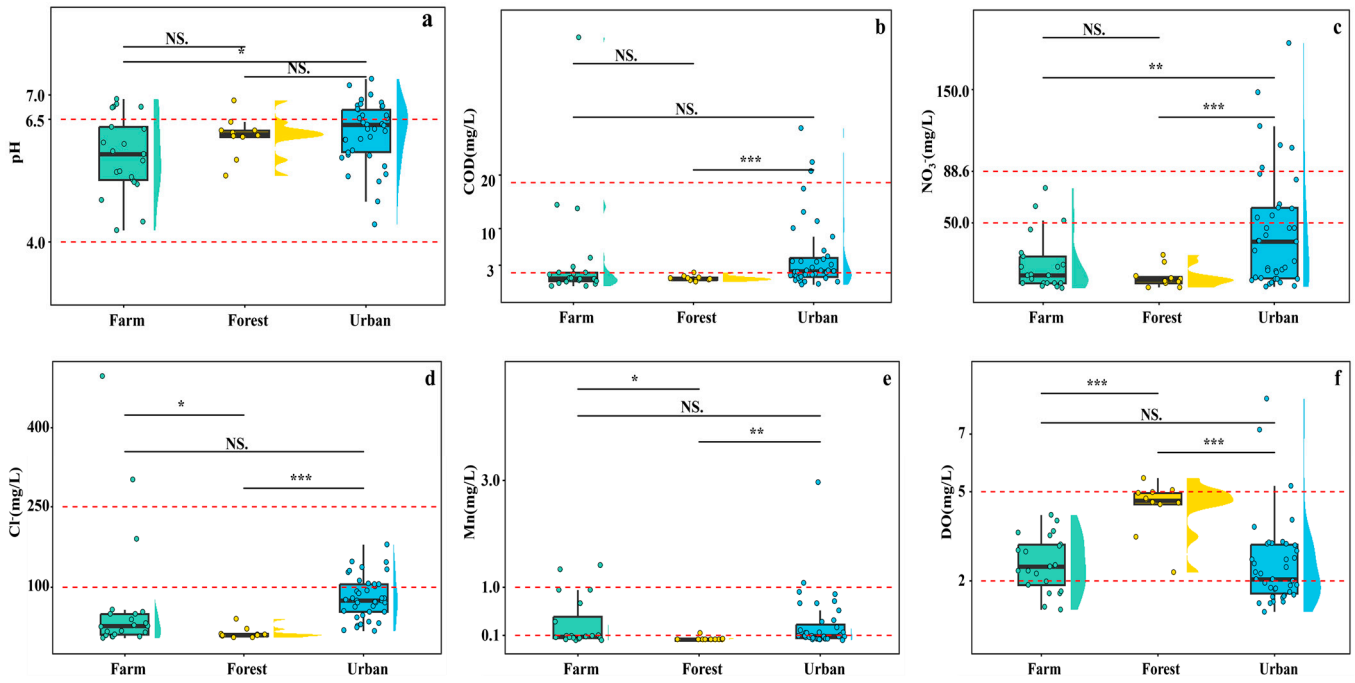

Figure 3. Comparison of Significant Differences in Hydrochemical Component Concentrations (**a**) pH; (**b**) COD; (**c**) NO_3^-; (**d**) Cl^-; (**e**) Mn; (**f**) DO. Note: *** denotes a p-value < 0.001; ** denotes a p-value < 0.01; * denotes a p-value < 0.1; NS: not significant. The red dash line represents the groundwater quality standard limit in China (GB/T 14848-2017) [23].

4.2. Mechanisms of Groundwater Hydrochemical Evolution in Rapidly Urbanizing Areas

4.2.1. Factors Controlling Groundwater Hydrochemistry

Gibbs diagrams are widely employed to qualitatively evaluate the relative influence of atmospheric precipitation, rock weathering, and evaporation–crystallization on the origin of dissolved ions in groundwater [32]. As shown in Figure 4, the majority of samples plot within the central region of the TDS versus $Na^+/(Na^+ + Ca^{2+})$ and $Cl^-/(Cl^- + HCO_3^-)$ fields, i.e., within the "rock-weathering" end-member domain. This distribution indicates that rock weathering reactions constitute the primary control on the major-ion composition of local groundwater. Nevertheless, a subset of samples collected beneath agricultural and forested land-use types falls into the precipitation-dominated sector, whereas several urban and agricultural samples shift toward the evaporation–crystallization quadrant, demonstrating that both rainfall inputs and evaporative concentration also modulate hydrochemical signatures. In addition, approximately 20% of the sampling sites lie outside the three conventional Gibbs sectors, implying an additional overprint of anthropogenic activities on the natural ionic assemblages. Zhou et al. also found that some sampling points were located outside the end-member range, indicating that human activities have had an impact on the groundwater chemistry [33].

4.2.2. Analysis of Hydrochemical Evolution Processes

To further elucidate the hydrochemical evolution of groundwater in the study area, ion-ratio analysis was employed to identify the dominant lithological weathering signatures and associated hydrogeochemical processes. Na-normalized molar ratios were first used to assign samples to specific weathering endmembers. Typical molar ratios for silicate weathering are $Ca^{2+}/Na^+ = 0.35 \pm 0.15$ and $Mg^{2+}/Na^+ = 0.24 \pm 0.12$; for carbonate weathering, 50 ± 20 and 20 ± 8; and for evaporite dissolution, 0.17 ± 0.09 and 0.02 ± 0.013. As shown in Figure 5a, most urban and agricultural plots cluster close to the silicate-evaporite join, whereas forested (and a minority of agricultural) samples shift toward the carbonate

field. This distribution reflects the regional aquifer lithology: shallow horizons are dominated by silicate rocks, with only minor carbonate outcrops whose dissolution imprint remains limited.

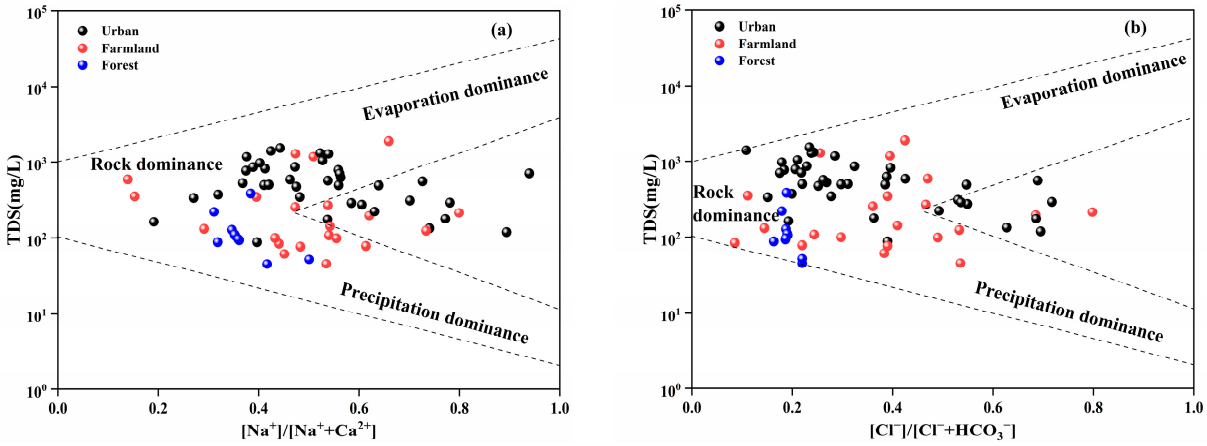

Figure 4. Identification plot of hydrochemical controls (**a**) $[Na^+]/[Na^+ + Ca^{2+}]$ vs. TDS; (**b**) $[Cl^-]/[Cl^- + HCO_3^-]$ vs. TDS.

When evaporite dissolution controls water chemistry, the molar ratio $Cl^-/(Na^+ + K^+)$ should equal unity (i.e., fall on the y = x line) [34]. In Figure 5b, 91.4% of the samples plot above this line, with $Na^+ + K^+$ significantly exceeding Cl^- and exhibiting a strong linear relationship (R^2 = 0.861). This indicates that silicate weathering constitutes the principal source of Na^+ and K^+, supplemented by minor evaporite dissolution. Moreover, urban samples display markedly higher $(Na^+ + K^+)$ relative to Cl^-, implying an additional anthropogenic contribution from industrial and domestic effluents [35].

The ratio of $[Ca^{2+} + Mg^{2+}]$ to $[HCO_3^- + SO_4^{2-}]$ can be used to determine the sources of Ca^{2+} and Mg^{2+}. A ratio greater than 1 indicates that Ca^{2+} and Mg^{2+} primarily originate from the dissolution of carbonate minerals. Conversely, a ratio of less than 1 suggests that these ions derive from the dissolution of sulfate or silicate minerals. When the ratio equals 1, it signifies that both carbonate and silicate rock weathering and dissolution are occurring simultaneously [36]. As depicted in Figure 5c, sample points from agricultural and forestry land primarily cluster around the y = x line, whereas those from urban land are concentrated below this line. The concentrations of $[Ca^{2+} + Mg^{2+}]$ and $[HCO_3^- + SO_4^{2-}]$ in urban land samples exceed those in agricultural and forestry land samples. This suggests that the weathering and dissolution of silicate rocks supply substantial amounts of $Ca^{2+} + Mg^{2+}$ to urban land water samples. In contrast, $Ca^{2+} + Mg^{2+}$ in agricultural and forestry land samples originate from the weathering and dissolution of both carbonate and silicate rocks. Additionally, acid rain (characterized by low pH values) is prevalent in the study area. This acid rain erodes surface carbonate rocks, which then recharge the shallow groundwater (with an average burial depth of 2.17 m). Consequently, the erosion and dissolution of carbonate rocks serve as the primary source of HCO_3^-.

The ratio plot of $[Ca^{2+}]/[SO_4^{2-}]$ can be used to assess the impact of evaporite weathering and dissolution on water chemistry [37]. As shown in Figure 5d, Ca^{2+} and SO_4^{2-} exhibit a strong linear relationship, indicating that evaporite weathering and dissolution are one of the sources of these ions. The sample points from all three types of land use are generally located above the y = x line, suggesting that there are additional sources contributing to the excess Ca^{2+}. As previously discussed, the weathering and dissolution of silicate rocks and the erosion of carbonate rocks also play significant roles in supplying Ca^{2+}.

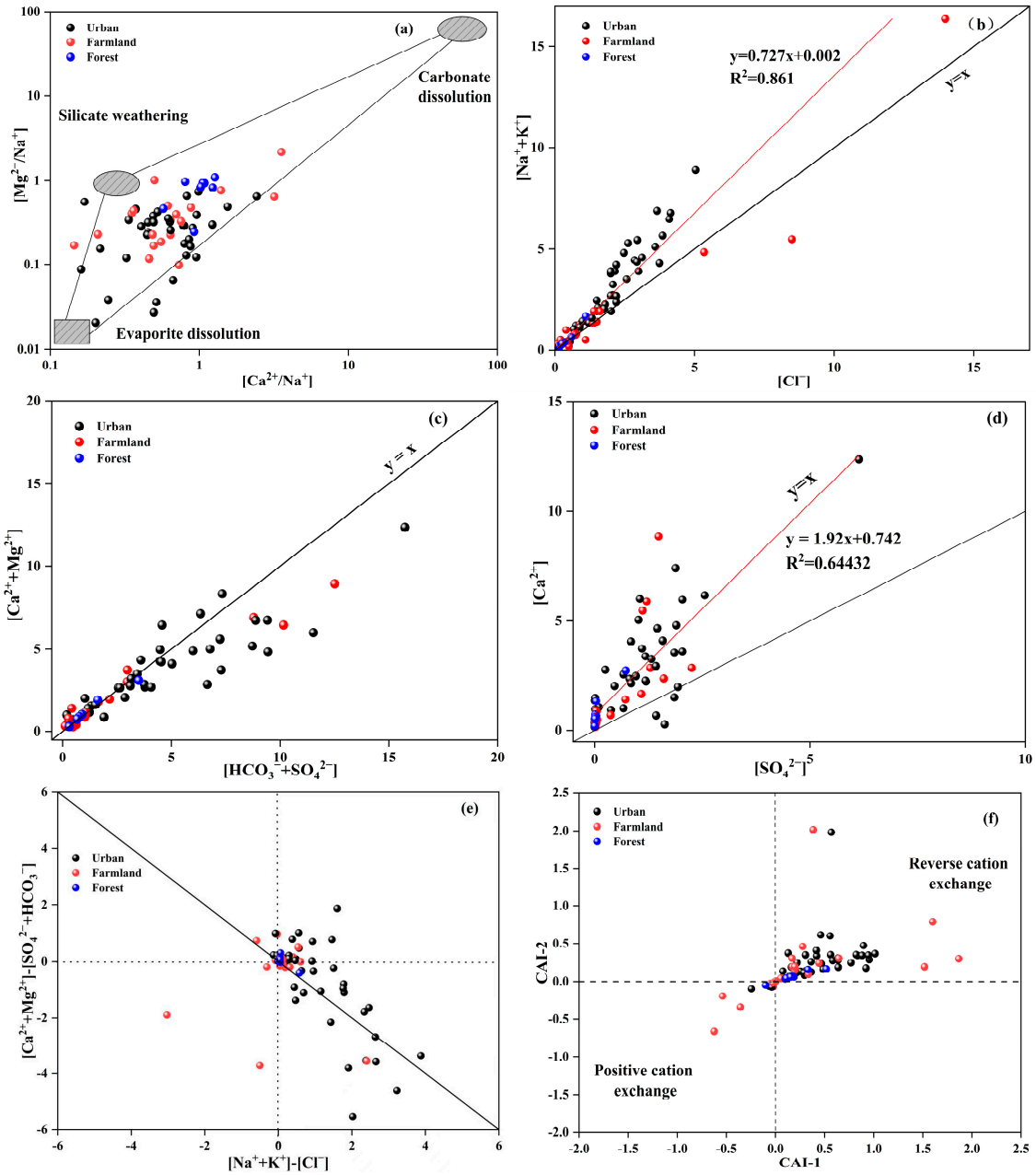

Figure 5. Ion ratio diagram: (**a**) [Ca^{2+}/Na^{+}] vs. [Mg^{2+}/Na^{+}]; (**b**) [Cl^{-}] vs. [Na^{+}]; (**c**) [HCO_3^{-} + SO_4^{2-}] vs. [Ca^{2+} + Mg^{2+}]; (**d**) [SO_4^{2-}] vs. [Ca^{2+}]; (**e**) [Na^{+} + K^{+}]-[Cl^{-}] vs. [Ca^{2+} + Mg^{2+}]-[HCO_3^{-} + SO_4^{2-}]; (**f**) CAI-1 vs. CAI-2.

To further illustrate the influence of hydrochemical processes on water chemistry, we examined cation exchange [38,39]. Figure 5e shows that all sample points cluster around the y = −x line, indicating that cation exchange is occurring. According to Figure 5f, more than 80% of the samples from each of the three land-use types fall in the CAI > 0 zone, demonstrating that reverse cation exchange dominates [40]. Combined with the preceding discussion, this indicates that the concentrations of Ca^{2+} and Mg^{2+} in the groundwater are jointly controlled by silicate weathering, carbonate dissolution, and reverse cation exchange.

4.2.3. Impact of Human Activities on Groundwater Hydrochemical Evolution

Human activities are also one of the significant factors influencing the hydrochemical evolution of groundwater. Typically, in regions with intense human activities, the concen-

trations of NO_3^-, Cl^-, SO_4^{2-}, and Na^+ in groundwater tend to increase markedly. Among these, SO_4^{2-} is mainly influenced by industrial activities, whereas NO_3^-, Cl^-, and Na^+ are affected by agricultural fertilization, manure, and domestic wastewater [41].

Based on the milliequivalent ratios of $[NO_3^-]/[Ca^{2+}]$ vs. $[SO_4^{2-}]/[Ca^{2+}]$, we can identify which type of human activity has impacted the groundwater [42]. When $[NO_3^-]/[Ca^{2+}] > [SO_4^{2-}]/[Ca^{2+}]$, groundwater is strongly influenced by agricultural activities or rainfall. Conversely, when $[NO_3^-]/[Ca^{2+}] < [SO_4^{2-}]/[Ca^{2+}]$, the impact of industrial activities is more pronounced. As shown in Figure 6, 61.5% of the sampling points are located in the mixed impact zone, indicating that the groundwater in the study area is affected by a combination of industrial wastewater, domestic sewage, and fertilizers. Zhang et al. also found that in rapidly urbanizing areas, groundwater is subjected to mixed contamination from industrial wastewater, domestic sewage, and landfill leachate [18]. The study area is a highly urbanized metropolis with a high population density and highly developed industry, resulting in a large volume of wastewater. The shallow groundwater level means that the discharge of domestic and industrial wastewater can directly affect the chemical composition of groundwater. Additionally, the frequent rainfall (with an annual precipitation of about 1900 mm) causes agricultural fertilizers to enter the groundwater through leaching and surface runoff, thereby causing groundwater pollution.

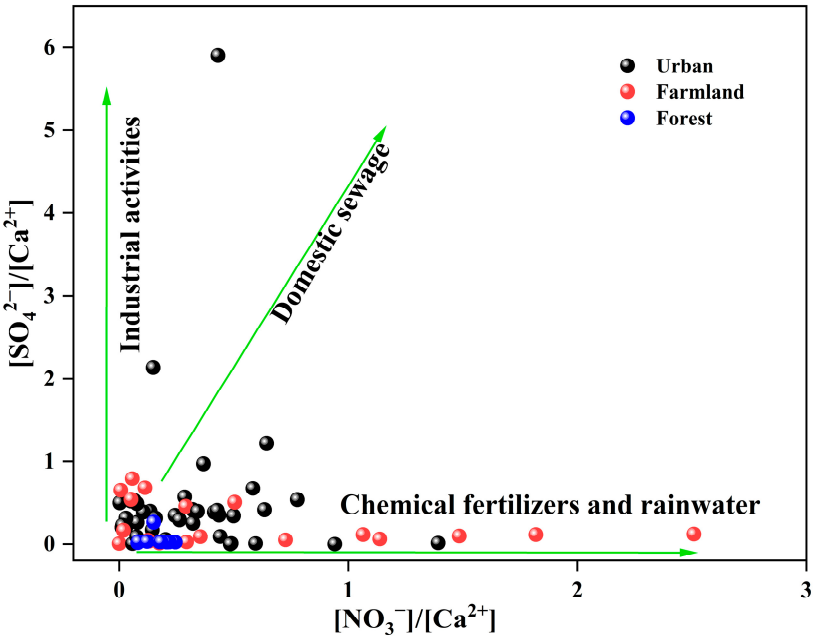

Figure 6. Identification plot of human activity impacts $[NO_3^-]/[Ca^{2+}]$ vs. $[SO_4^{2-}]/[Ca^{2+}]$.

4.3. Source Apportionment of Groundwater Quality Pollution in Rapidly Urbanizing Areas

4.3.1. Pollution Source Apportionment Based on the PMF Model

In this study, the PMF model was employed to quantitatively identify the sources of groundwater pollution in the study area. Concentration data and uncertainty data for 17 hydrochemical indicators (K^+, Na^+, Ca^{2+}, Mg^{2+}, Cl^-, SO_4^{2-}, HCO_3^-, NO_3^-, NO_2^-, NH_4^+, COD, TH, TDS, Fe, and Mn) from 70 groundwater samples were input into the PMF model. After running the model, we iteratively adjusted the "strong" and "weak" settings for elements and the factor format to optimize the fit. The goal was to achieve a fitting coefficient greater than 0.5 for the measured versus simulated element concentrations and a difference of less than 10% between the calculated Q value and the theoretical Q value. Ultimately, a three-factor solution was determined to be the optimal configuration.

As shown in Table 3, factor 1 accounts for 43.9% of the total variance and is heavily weighted by NH_4^+, NO_2^-, Cl^-, SO_4^{2-}, HCO_3^-, TH, COD, Ca^{2+}, Fe, and Mn; NO_3^- also displays moderately high loading. NH_4^+ and NO_3^- in shallow aquifers are typically derived from domestic sewage, chemical fertilizers, soil organic nitrogen, and atmospheric deposition [43], whereas Cl^- originates from halite dissolution, wastewater, seawater intrusion, or road-de-icing salts [44]. The mean water-table depth (2.17 m) is shallow, and most sampling wells are large-diameter domestic wells located within villages; thus, untreated domestic effluent can readily infiltrate. COD, a proxy for organic and reduced-matter contamination, exhibits an exceedance rate of 44.3%, indicating prominent organic pollution. Previous study indicates that COD is supplied by domestic and industrial effluents, agricultural runoff, urban stormwater, natural organic matter, and landfill leachate [45]. Fe and Mn are additionally introduced by industrial discharges (mining, steel making, electroplating) and corroded municipal pipelines. Shenzhen's leading industries—electronics, high-end equipment manufacturing, metal products, general machinery, and automotive production—generate large volumes of processed wastewater that, if inadequately treated, can readily contaminate the shallow aquifer. In addition, the concentrations of Fe and Mn in groundwater range from 0 to 11.5 mg/L and from 0.003 to 2.96 mg/L, respectively, with high spatial variability and high exceedance rates, indicating that they are affected by human activities (such as industrial wastewater). Therefore, Factor 1 is designated "sewage and industrial pollution". Source-contribution analysis indicates that this factor supplies 51.0% of NH_4^+, 65.1% of NO_2^-, 53.6% of Cl^-, 59.0% of SO_4^{2-}, 60.6% of HCO_3^-, 58.6% of TH, 55.3% of COD, 49.9% of Ca^{2+}, 75.6% of Fe, and 56.3% of Mn (Figure 7).

Table 3. Source profiles obtained from the PMF model.

Parameters	Factor 1	Factor 2	Factor 3
pH	2.04	2.60	1.36
DO	0.773	1.55	0.005
NO_3^-	0.0009	0	0.003
NH_4^+	0.00004	0.00001	0.00003
NO_2^-	0.010	0.003	0.002
Cl^-	7.50	4.66	1.82
SO_4^{2-}	0.0008	0.0006	0
COD	1.11	0.596	0.3
TDS	12.8	46.2	30.8
TH	21.4	10.7	4.41
HCO_3^-	11.4	1.55	5.85
K^+	0.006	1.05	0.207
Na^+	0.692	3.35	1.64
Ca^{2+}	4.00	2.93	1.08
Mg^{2+}	0	0.681	0.375
Fe	0.00006	0	0.00002
Mn	0.005	0.004	0.001
Possible sources	Sewage and and industrial pollution	Water–rock interaction	Agricultural fertilizer
Contribution (%)	43.9	37.0	19.1

Factor 2 explains 37.0% of the variance and is dominated by pH, DO, TDS, K^+, Na^+ and Mg^{2+}. Na^+, K^+, Mg^{2+}, and TDS are released primarily by water–rock interaction [46], whereas pH and DO are bulk physicochemical parameters that reflect the integrated outcome of aqueous chemical and biological processes rather than specific pollutant sources [47]. As analyzed in Section 4.2.2, the K^+, Na^+, and Mg^{2+} in the groundwater

of the study area mainly originate from the weathering and dissolution of rocks. Thus, Factor 2 is consequently interpreted as "water–rock interaction". According to Figure 7, this factor contributes 43.6% of pH, 66.6% of DO, 51.3% of TDS, 83.1% of K^+, and 64.5% of Na^+.

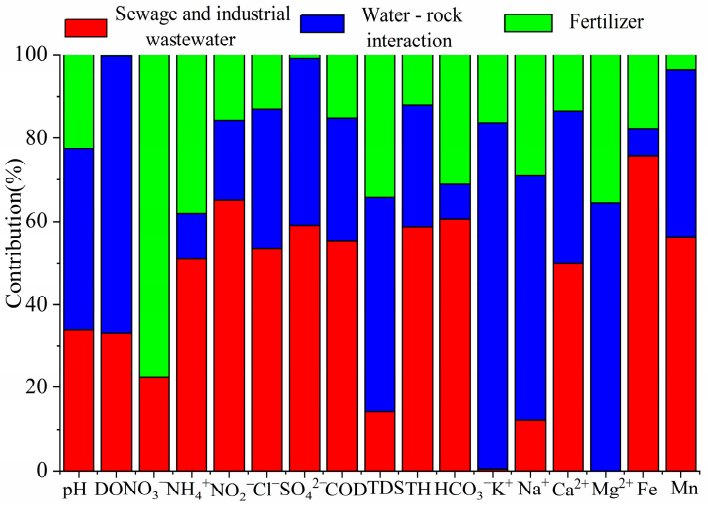

Figure 7. Contribution rates of groundwater pollution sources.

Factor 3 accounts for 19.1% of the variance and is heavily loaded on NO_3^-, with secondary contributions from NH_4^+, TDS, and Na^+. As discussed earlier, NO_3^- and NH_4^+ are introduced by chemical fertilizers, sewage, rain, etc. Because the concentration of NO_3^- in rain is low (1.47 mg/L) [25], and PC1 and PC3 are independent of each other. Due to PC1 represents sewage, therefore, Factor 3 is assigned to "agricultural fertilizer". Figure 7 shows that this source contributes 77.5% of NO_3^-, 38.1% of NH_4^+, 34.3% of TDS, and 28.9% of Na^+.

4.3.2. Spatial Distribution of Pollution Sources

Spatial interpolation of the factor scores for the three PMF-derived sources (PC1–PC3) was conducted to generate distribution maps of groundwater contamination across Shenzhen (Figure 8).

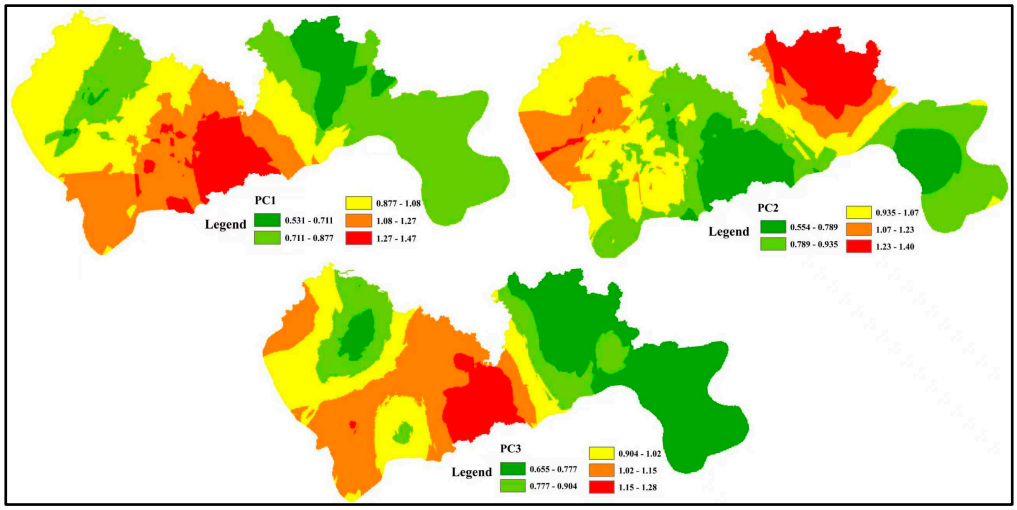

Figure 8. Spatial Distribution of Groundwater Pollution Sources.

High PC1 scores are concentrated around the peripheral districts of the central metropolitan area, indicating severe impacts from domestic sewage and industrial ef-

fluence. These peri-urban zones are densely populated and host numerous small-scale factories that often lack wastewater-treatment facilities; consequently, uncontrolled discharge constitutes the principal threat to groundwater quality. Elevated PC2 scores occur mainly in the north-eastern and north-western parts of the study area, reflecting regions where water–rock interaction governs the hydrochemical signature. High PC3 scores are observed southeast of the city core, demonstrating that intensive agricultural activity—and associated fertilizer use—is the dominant driver of nitrate contamination in that sector.

Overall, the spatial pattern of pollution sources is tightly coupled to land–use type. In highly urbanized districts, groundwater quality is controlled primarily by municipal and industrial wastewater; therefore, comprehensive collection and treatment of all sewage streams is the critical measure for preventing further deterioration. In agricultural areas, excessive fertilizer application is the key factor, so strict control of diffuse agricultural inputs is essential for groundwater protection.

5. Limitations of the Study

This study combined hydrochemical characterization with the PMF model to quantify and visualize groundwater pollution sources in a rapidly urbanizing area, thereby providing environmental managers with a clear basis for targeted control strategies. Nevertheless, three main limitations should be acknowledged:

(1) Sampling frequency was low; samples were collected only during the wet season. Consequently, temporal variability in groundwater quality and potential seasonal shifts in contaminant sources could not be resolved. In addition, due to confidentiality issues regarding the maps, we were unable to obtain high-precision land-use type maps for the study area. Consequently, we could not acquire the distances between sampling wells and specific human activity sites such as industrial parks, wastewater treatment plants, drainage networks, and landfills. This limitation prevented us from accurately analyzing the relationship between specific human activities and groundwater pollution.

(2) Although PMF successfully apportioned overall contaminant loads, the accuracy of source attribution could be further improved. In recent years, dual-isotope techniques (e.g., δ^{15} N and δ^{18} O of NO_3^-; δ^{34} S and δ^{18} O of SO_4^{2-}) coupled with receptor models have markedly refined source quantification for specific solutes [48,49]. Owing to budget constraints, such isotopic analyses were not conducted in the present work.

(3) The investigation generated an extensive hydrochemical data set, but background hydrogeochemical information remains incomplete. As a result, advanced machine learning algorithms (e.g., Random Forest) that could identify key drivers of water-quality degradation and predict future trends were not employed.

Future research should therefore: (i) implement high-frequency sampling campaigns covering both wet and dry seasons, (ii) integrate multi-isotope tracers with PMF or other receptor models, and (iii) apply machine learning approaches to achieve more robust source apportionment and predictive capability for groundwater quality in rapidly urbanizing regions.

6. Conclusions

This study has provided valuable insights into the hydrochemical evolution and pollution sources of groundwater in highly urbanized regions, using Shenzhen, China, as a case study. By employing a combination of multivariate statistical techniques and the Positive Matrix Factorization (PMF) model, we have elucidated the complex interactions between human activities and groundwater quality. The main conclusions of this study are as follows:

(1) The groundwater quality in highly urbanized areas shows a high exceedance rate of water quality parameters, with the exceedance rates of pH, NH_4^+, COD, Mn, and Fe being 67.1%, 44.3%, 44.3%, 34.3% and 31.4%, respectively. The Water Quality Index assessment revealed that 32.9% of the groundwater samples were classified as poor, underscoring the substantial impact of human activities on groundwater quality. Land-use types significantly affected groundwater quality; the concentration of COD, NO_3^-, Mn, and Fe in the urban areas were significantly higher than in the agricultural and forested areas.

(2) Rock weathering is the primary control on the groundwater chemistry in the region, and human activities also have an important impact on the formation of groundwater chemistry. Among them, silicate weathering constitutes the principal source of Na^+ and K^+, while Ca^{2+}, Mg^{2+} and HCO_3^- primarily originate from the dissolution of carbonate minerals. Moreover, the weathering and dissolution of evaporites are one of the main sources of SO_4^{2-}. In addition, domestic sewage, industrial wastewater, and fertilizers are the main sources of NO_3^- in the groundwater of the region.

(3) The PMF model identified three major pollution sources: domestic and industrial wastewater (43.9%), enhanced water–rock interactions (37.0%), and agricultural fertilizers (19.1%). Geostatistical spatial interpolation techniques further demonstrated that groundwater quality in urban areas is primarily controlled by the discharge of domestic and industrial wastewater, while in agricultural areas, excessive fertilizer application is the main driver of groundwater degradation. Therefore, future research should advocate for strict control and compliance policies for municipal sewage discharge, as well as optimize agricultural fertilization strategies, such as formula fertilization and the use of slow-release fertilizers, to prevent further deterioration of groundwater quality.

Although this study identified groundwater pollution sources in highly urbanized regions, it faced several limitations: low sampling frequency restricted to the wet season, lack of isotopic analyses due to budget constraints, and incomplete background data that hindered the application of advanced machine learning techniques. Future work should include year-round high-frequency sampling, the integration of multi-isotope tracers with PMF, and the application of machine learning methods to enhance source apportionment and predictive capabilities, thereby supporting improved groundwater management in urban areas.

Supplementary Materials: The following supporting information can be downloaded at: https://www.mdpi.com/article/10.3390/w17202945/s1. Table S1: Hydrochemical parameters, analytical method, equipment and detection limits; Table S2: Table of weight values for groundwater chemistry indicators.

Author Contributions: Y.W.: Investigation, methodology, software, data curation, and writing—original draft preparation. Y.L.: Investigation, software, and methodology. L.Z.: Investigation, methodology, and software. C.L.: Investigation, methodology, and data curation. Q.M.: Investigation and methodology. J.Y.: Supervision, methodology, and writing—reviewing and editing. L.W.: Investigation and methodology. All authors have read and agreed to the published version of the manuscript.

Funding: This research received no external funding.

Data Availability Statement: The original contributions presented in this study are included in the article/Supplementary Material. Further inquiries can be directed to the corresponding author.

Acknowledgments: The authors gratefully acknowledge the editor and anonymous reviewers for their valuable comments on this manuscript. The authors also appreciate financial support from the different organizations.

Conflicts of Interest: The authors declare no conflicts of interest.

References

1. Peng, H.Q.; Yang, W.; Ferrer, A.; Xiong, S.; Li, X.; Niu, G.; Lu, T. Hydrochemical characteristics and health risk assessment of groundwater in karst areas of southwest China: A case study of Bama, Guangxi. *J. Clean. Prod.* **2022**, *341*, 130872. [CrossRef]
2. Zhang, Q.Q.; Wang, H.W.; Xu, Z.; Li, G.; Yang, M.N.; Liu, J. Quantitative identification of groundwater contamination sources by combining isotope tracer technique with PMF model in an arid area of northwestern China. *J. Environ. Manag.* **2023**, *325*, 116588. [CrossRef]
3. Panneerselvam, B.; Muniraj, K.; Duraisamy, K.; Pande, C.; Karuppannan, S.; Thomas, M. An integrated approach to explore the suitability of nitrate-contaminated groundwater for drinking purposes in a semiarid region of India. *Environ. Geochem. Health* **2023**, *45*, 647–663. [CrossRef]
4. Hasan, M.S.U.; Rai, A.K. Groundwater quality assessment in the Lower Ganga Basin using entropy information theory and GIS. *J. Clean. Prod.* **2020**, *274*, 123077. [CrossRef]
5. Wang, L.; Zhang, Q.Q.; Wang, H.W. Rapid urbanization has changed the driving factors of groundwater chemical evolution in the large groundwater depression funnel area of northern China. *Water* **2023**, *15*, 2917. [CrossRef]
6. Torres-Martínez, J.A.; Mora, A.; Knappett, P.S.K.; Ornelas-Soto, N.; Mahlknecht, J. Tracking nitrate and sulfate sources in groundwater of an urbanized valley using a multi-tracer approach combined with a Bayesian isotope mixing model. *Water Res.* **2020**, *182*, 115962. [CrossRef]
7. Wang, F.; Liu, L.; Xu, W.; Li, Y.; Ruan, Q.; Cao, W. Multiple stable isotopic approaches for tracing nitrate contamination sources: Implications for nitrogen management in complex watersheds. *Ecotoxicol. Environ. Safe* **2024**, *269*, 115822. [CrossRef] [PubMed]
8. Li, Y.; Tu, Y.; Sun, T.; Duan, Y.; Kou, J.; Li, W.; Gao, J. Source apportionment of organic carbon and nitrogen in sediments from river and lake in the highly urbanized Changjiang Delta. *J. Hazard. Mater.* **2024**, *478*, 135590. [CrossRef] [PubMed]
9. Li, X.; Liang, G.; He, B.; Ning, Y.; Yang, Y.; Wang, L.; Wang, G. Recent advances in groundwater pollution research using machine learning from 2000 to 2023: A bibliometric analysis. *Environ. Res.* **2025**, *267*, 120683. [CrossRef]
10. Wang, L.; Wang, Q.; Zheng, D. Study on the pollution mechanism and driving factors of groundwater quality in typical industrial areas of China. *Water* **2025**, *17*, 1420. [CrossRef]
11. Marazuela, M.Á.; Jiménez, J.; Baquedano, C.; Martínez-León, J.; Gasco-Cavero, S.; Cruz-Pérez, N.; Santamarta, J.C.; Garcia-Gil, A. Hydrogeological and hydrochemical processes affecting groundwater quality on volcanic islands: Insights from El Hierro (Canary Islands, Spain). *J. Hydrol.* **2025**, *654*, 132874. [CrossRef]
12. Khaskheli, A.; Khuhawar, T.M.J.; Khuhawar, M.Y.; Khuhawar, F.Y.; Lanjwani, M.F.; Landar, A.Q. Evaluation of groundwater quality of Mirpurkhas District, Sindh, Pakistan, for drinking, irrigation and multivariate analysis. *Arab. J. Geosci.* **2025**, *18*, 136. [CrossRef]
13. Deng, Y.; Lu, Y.; Du, X.; Ye, X.; Feng, J. Identifying spatial patterns and driving factors of anthropogenic impacts on the groundwater environment based on groundwater chemical kinetics. *J. Clean. Prod.* **2025**, *486*, 144436. [CrossRef]
14. Wang, Q.; Ou, X.; Wu, C.; Yao, S.; Huang, S.; Zhu, C.; Liao, Z.; Wang, K.; Zhang, S.; Chen, J. Machine learning-driven PMF modeling for accurate and objective source identification of VOCs. *Atmos. Pollut. Res.* **2025**, 102721. [CrossRef]
15. Lv, X.; Li, C.; Wang, H.; Yang, S.; Wang, S.; Yang, C.; Teng, F.; Zhao, J.; Xu, X.; Zhang, H.; et al. Source apportionment and risk quantification of soil heavy metals using SOM-PMF model: Implications for ecological and human health management. *Environ. Monit. Assess.* **2025**, *197*, 868. [CrossRef]
16. Liu, Z.; Wang, L.; Yan, M.; Ma, B.; Cao, R. Source apportionment of soil heavy metals based on multivariate statistical analysis and the PMF model: A case study of the Nanyang Basin, China. *Environ. Technol. Innov.* **2024**, *33*, 103537. [CrossRef]
17. Wang, A.; Wang, J.; Luan, B.; Wang, S.; Yang, D.; Wei, Z. Classification of pollution sources and their contributions to surface water quality using APCS-MLR and PMF model in a drinking water source area in southeastern China. *Water* **2024**, *16*, 1356. [CrossRef]
18. Zhang, Q.Q.; Miao, L.; Wang, H.W.; Hou, J.; Li, Y. How rapid urbanization drives deteriorating groundwater quality in a provincial capital of China. *Pol. J. Environ. Stud.* **2020**, *29*, 441–450. [CrossRef]
19. Attard, G.; Winiarski, T.; Rossier, Y.; Eisenlohr, L. Impact of underground structures on the flow of urban groundwater. *J. Hydrol.* **2016**, *24*, 5–19. [CrossRef]
20. Ruan, D.; Bian, J.; Wang, Y.; Wu, J.; Gu, Z. Identification of groundwater pollution sources and health risk assessment in the Songnen Plain based on PCA-APCS-MLR and trapezoidal fuzzy number-Monte Carlo stochastic simulation model. *J. Hydrol.* **2024**, *632*, 130897. [CrossRef]
21. Jiang, Z.; Wang, C.; Liu, Y.; Feng, Z.; Ji, C.; Zhang, H. Study on the raw water allocation and optimization in Shenzhen city, China. *Water* **2019**, *11*, 1426. [CrossRef]
22. Zhang, Q.Q.; Sun, J.; Liu, J.; Huang, G.; Lu, C.; Zhang, Y. Driving mechanism and sources of groundwater nitrate contamination in the rapidly urbanized region of south China. *J. Contam. Hydrol.* **2015**, *182*, 221–230. [CrossRef] [PubMed]
23. *GB/T 14848-2017*; Standard for Groundwater Quality. Ministry of Natural Resources of the People's Republic of China: Beijing, China, 2017.

24. World Health Organization. *Guidelines for Drinking-Water Quality*, 4th ed.; World Health Organization: Geneva, Switzerland, 2011.
25. Zhou, X.; Xu, Z.; Liu, W.; Wu, Y.; Zhao, T.; Jiang, H.; Zhang, X.; Zhang, J.; Zhou, L.; Wang, Y. Chemical composition of precipitation in Shenzhen, a coastal mega-city in South China: Influence of urbanization and anthropogenic activities on acidity and ionic composition. *Sci. Total Environ.* **2019**, *662*, 218–226. [CrossRef] [PubMed]
26. Zhang, Q.Q.; Wang, H.W.; Wang, Y.C.; Yang, M.N.; Zhu, L. Groundwater quality assessment and pollution source apportionment in an intensely exploited region of northern China. *Environ. Sci. Pollut. Res.* **2017**, *24*, 16639–16650. [CrossRef]
27. Wang, Q.; Wang, M.; Li, Y.; Guo, B.; Li, H.; Liu, Y.; Zhao, L.; Ma, C.; Yuan, Z. Study on Natural Background Levels and Mechanisms of Groundwater Contamination in an Overexploited Aquifer Region: A Case Study of Xingtai City, North China Plain. *Water* **2025**, *17*, 2836. [CrossRef]
28. Wang, L.; Yang, N.; Zhao, Y.; Zhang, Q. Research on the Features and Driving Factors of Shallow Groundwater Quality in Arid Areas, Northwest China. *Water* **2025**, *17*, 934. [CrossRef]
29. Rai, S.C.; Saha, A.K. Impact of urban sprawl on groundwater quality: A case study of Faridabad city, National Capital Region of Delhi. *Arab. J. Geosci.* **2015**, *8*, 8039–8045. [CrossRef]
30. Lockhart, K.; King, A.; Harter, T. Identifying sources of groundwater nitrate contamination in a large alluvial groundwater basin with highly diversified intensive agricultural production. *J. Contam. Hydrol.* **2013**, *151*, 140–154. [CrossRef]
31. Zhang, Q.Q.; Wang, H.W. Assessment of sources and transformation of nitrate in the alluvial–pluvial fan region of north China using a multi-isotope approach. *J. Environ. Sci.* **2020**, *89*, 9–22. [CrossRef]
32. Shi, X.; Gao, Y.; Qian, H.; Chen, J.; Li, W.; Li, S.; Liu, Y. Elucidating the hydrochemistry and REE evolution of surface water and groundwater affected by acid mine drainage. *Environ. Pollut.* **2025**, *366*, 125495. [CrossRef]
33. Zhou, B.; Wang, H.W.; Zhang, Q.Q. Assessment of the evolution of groundwater chemistry and its controlling factors in the Huangshui River Basin of northwestern China, using hydrochemistry and multivariate statistical techniques. *Int. J. Environ. Res. Public Health* **2021**, *18*, 7551. [CrossRef] [PubMed]
34. Sun, R.; Zhang, X.Q.; Wu, Y.H. Major ion chemistry of water and its controlling factors in the Yamzhog Yumco basin, south Tibet. *J. Lake Sci.* **2012**, *24*, 600–608. [CrossRef]
35. Sun, H.; Huffine, M.; Husch, J.; Sinpatanasakul, L. Na/Cl molar ratio changes during a salting cycle and its application to the estimation of sodium retention in salted watersheds. *J. Contam. Hydrol.* **2012**, *136*, 96–105. [CrossRef] [PubMed]
36. Yang, J.; Zhao, W.; Liang, X.; Xu, F. The hydrochemical characteristics and formation mechanism of highly mineralized coal mine water in semi-arid regions in northwest China. *Water* **2024**, *16*, 2244. [CrossRef]
37. Shen, B.; Wu, J.; Zhan, S.; Jin, M.; Saparov, A.S.; Abuduwaili, J. Spatial variations and controls on the hydrochemistry of surface waters across the Ili–Balkhash Basin, arid Central Asia. *J. Hydrol.* **2021**, *600*, 126565. [CrossRef]
38. Lakhdari, A.S.; Bouselsal, B.; Saibi, H.; Ouarekh, M. Assessment of groundwater quality and hydrogeochemical properties in the adrar continental intercalaire aquifer of the Algerian Sahara. *Appl Water Sci.* **2025**, *15*, 175. [CrossRef]
39. Boualem, B.; Egbueri, J.C. Graphical, statistical and index-based techniques integrated for identifying the hydrochemical fingerprints and groundwater quality of in Salah, Algerian Sahara. *Environ. Geochem. Health* **2024**, *46*, 158. [CrossRef]
40. Bouselsal, B.; Satouh, A.; Egbueri, J.C. Evaluating water quality, mineralization mechanisms, and potential health risks of nitrate contamination in the Continental Intercalaire aquifer of Reggane, Algeria. *Environ. Earth Sci.* **2024**, *83*, 539. [CrossRef]
41. Saccon, P.; Leis, A.; Marca, A.; Kaiser, J.; Campisi, L.; Böttcher, M.E.; Savarino, J.; Escher, P.; Eisenhauer, A.; Erbland, J. Multi-isotope approach for the identification and characterisation of nitrate pollution sources in the Marano lagoon (Italy) and parts of its catchment area. *Appl. Geochem.* **2013**, *34*, 75–89. [CrossRef]
42. Jiang, W.; Li, B.; Zhang, Z.; Zhang, Y. Hydrochemical characteristics, controlling factors and groundwater sources of Zaozigou gold mine. *Sustainability* **2024**, *16*, 7989. [CrossRef]
43. Wu, Y.; Ju, H.; Jiang, H.; Zhang, G.; Qi, P.; Li, Z. Identifying nitrate sources and transformations in an agricultural watershed in Northeast China: Insights from multiple isotopes. *J. Environ. Manag.* **2023**, *340*, 118023. [CrossRef] [PubMed]
44. Jin, Z.; Xue, Q.; Chen, L.; Jin, M.; Li, F. Using dual isotopes to evaluate sources and transformations of nitrate in the West Lake watershed, eastern China. *J. Contam. Hydrol.* **2015**, *177–178*, 64–75. [CrossRef]
45. Lee, J.; Lee, S.; Yu, S.; Rhew, D. Relationships between water quality parameters in rivers and lakes: BOD5, COD, NBOPs, and TOC. *Environ. Monit. Assess.* **2016**, *188*, 252. [CrossRef]
46. Fan, W.; Zhou, J.; Zheng, J.; Guo, Y.; Hu, L.; Shan, R. Hydrochemical characteristics, control factors and health risk assessment of groundwater in typical arid region Hotan Area, Chinese Xinjiang. *Environ. Pollut.* **2024**, *363*, 125301. [CrossRef]
47. Xiao, J.; Jin, Z.D.; Wang, J.; Zhang, F. Hydrochemical characteristics, controlling factors and solute sources of groundwater within the Tarim River Basin in the extreme arid region, NW Tibetan Plateau. *Quat. Int.* **2015**, *380*, 237–246. [CrossRef]

48. Ji, X.; Shu, L.; Chen, W.; Chen, Z.; Shang, X.; Yang, Y.; Dahlgren, R.A.; Zhang, M. Nitrate pollution source apportionment, uncertainty and sensitivity analysis across a rural–urban river network based on $\delta^{15}N/\delta^{18}O$–$NO_3^-$ isotopes and SIAR modeling. *J. Hazard. Mater.* **2022**, *438*, 129480. [CrossRef]
49. Jung, H.; Kim, J.; Lee, J. Seasonal and spatial contributions of sulfate and trace elements in river water in mining districts: Insights from hydrogeochemical and isotopic analysis based on statistical models. *J. Hazard. Mater.* **2025**, *488*, 137246. [CrossRef] [PubMed]